



Novel Automated Method for Minirhizotron Image Analysis: Root Detection using Curvelet Transform

H. Rahmanzadeh^a, S. V. Shojaedini^{*b}

^a Department of Electrical, Biomedical and Mechatronics Engineering, Qazvin Branch, Islamic Azad University, Qazvin, Iran.

^b Department of Electrical Engineering and Information Technology, Iranian Research Organization for Science and Technology, Iran.

PAPER INFO

Paper history:

Received 06 December 2015

Received in revised form 14 February 2016

Accepted 03 March 2016

Keywords:

Minirhizotron Images

Root Detection

Curvelet Sub-Bands

Mapping Function

ABSTRACT

In this article a new method is introduced for distinguishing roots and background based on their digital curvelet transform in minirhizotron images. In the proposed method, the nonlinear mapping is applied to sub-band curvelet components followed by boundary detection using energy optimization concept. The curvelet transform has the excellent capability in detecting roots with different orientations and contrasts, thanks to its better sparse representation and more directionality feature than existing approaches. Furthermore, adapting the parameters of the mapping function due to curvelet coefficients is very beneficial for magnifying weak ridges as well as better compatibility with different minirhizotron images. Performance of the proposed method is evaluated on several minirhizotron images in two different scenarios. In the first scenario, images contain several roots, while the second scenario belongs to no-root images, which increases the chance of false detections. The results show that the detection rate of the proposed method is 4 to 27 percent better than its alternatives, in presence of zero false detection. Furthermore, it is shown that better characterization of roots by proposed algorithm does not lead to extract more false objects compared to the results of the other examined algorithms.

doi: 10.5829/idosi.ije.2016.29.03c.08

1. INTRODUCTION

Roots are one of the most important parts of plants which serve several important functions such as supporting the above ground portion and providing water and nutrients. Studying the length, diameter and associated surface area of the root may help researchers to monitor the growth procedure of plants. Furthermore, this study may improve our understanding of root dynamics and associated functions in ecological systems [1]. Unfortunately, there are some shortcomings in in-situ viewing of roots. The main problem is that unlike the above ground plant components, roots are included in the soil [2].

For many decades, the soil core sampling has been the most common method for investigating the root. This method is based on cleaned root samples which are obtained after operations like washing from soil coring.

*Corresponding Author's Email: shojadini@irost.ir (S. V. Shojaedini)

Although, this method may provide exact information of root parameters but, it is time consuming and destructive [3].

Today, non-destructive equipment like rhizotrons and minirhizotrons were developed for the observation and analysis of root growth. Rhizotrons are large underground laboratories which are composed of transparent-wall chambers for studying roots in soil without core sampling. They use special imaging devices for observation of root morphology and analysis of its growth while the above parts of the plant are exposed to natural conditions. Rhizotrons have several disadvantages such as being expensive to construct and maintain [4], so a very limited number of Rhizotrons have been built world-wide. Therefore, they have been replaced by minirhizotron systems which are combination of imaging device and transparent plastic tubes that are buried in the soil near the plants.

Minirhizotrons, thereby allow repeated in-situ observations and analysis with minimum disturbance to the agricultural and pristine ecosystems. In the early

years, the minirhizotron image analysis was conducted by using manual procedures which will give detailed information on root production and mortality. Unfortunately, this method is labor-intensive and time-consuming. Therefore, the automated image analysis has been substituted for data processing [5]. The automated analysis encounter with several challenges like low contrast of minirhizotron images, existing bright objects in images which may be detected as roots and finally the possibility of changing brightness at different parts of the root. The above factors may lead to serious problems in root analysis such as root splitting or merging, increasing false positives and decrease detection rate which limit the performance of the automated methods.

In some researches the global and local thresholding have been applied for detecting root [6]. Unfortunately, the correct roots are not extracted by these methods because non-root objects have the same intensity distribution as the roots and the resultant histograms are not bimodal.

Some other methods utilize gray level co-occurrence matrix and local entropy thresholding to detect roots. The results show that this group of methods has a great ability in detecting young roots which are usually lighter in color [7]. Another family of algorithms tries to improve the performances of the above mentioned methods by using boosting classifiers. These approaches are based on incorporation of five concepts consisting of gray level histogram distribution, interior intensity edges, eccentricity and approximate line symmetry and boundary parallelism [8]. Unfortunately, these algorithms are not able to detect those roots which have not enough lighting and usual shape.

In other approaches artificial neural networks have been used to detect roots in minirhizotron images. Using neural networks has excellent results to identify roots in the training images. However, there is a significant decrease in detection rate when this method is applied to images on which it had not been trained [9].

In some methods the root detection in minirhizotron images is modeled as a Gibbs point process [10]. In these methods root segments are formed using grouping seed points into part linear structures followed by combination and validation schemes. After root center lines are found, root regions have been detected by using recursively bottom-up region growing method.

In some recent studies the energy functions are used for root detection. In such methods, the foreground of minirhizotron image is separated from its background by optimizing the energy function [11]. This method has better ability than threshold-based approaches in detecting roots in low contrast minirhizotron image, because of its independence to histogram of image.

In this paper, a new method is introduced for separating root from other parts in minirhizotron images. In the proposed method, firstly the digital

curvelet transform is applied to the image under test to obtain a better sparse representation and more directionality feature. Furthermore, this approach performs better handling of singularities in image under test than its original form and other available multi scale transforms. In the next step, the curvelet sub-bands are mapped by using a nonlinear function to magnify the weak ridges of the roots. Finally, the boundaries of the roots are determined by utilizing energy function concept which had led to acceptable results in our previous research [11].

The paper is organized as follows. In Section 2, the proposed algorithm is introduced including digital estimation of curvelet transform via Unequally Spaced Fast Fourier Transform (USFFT) followed by the root detection scheme. In Section 3, the performance of the proposed method is evaluated on several minirhizotron images. In Section 4, the results from experiments are compared with those of several existing methods by using some effective parameters. Conclusion is presented in the last section of the paper.

2. MATHEMATICAL MODEL

Suppose I is a minirhizotron image which includes root, soil and non-root objects. Soil and non-root objects is called background in this paper. For each pixel of I it may be written:

$$I_{mn} = I(m, n) \quad 1 \leq m \leq M \quad 1 \leq n \leq N \quad (1)$$

In the above equation, I_{mn} is brightness value of a pixel which is located in row m and column n , further (M, N) are image sizes.

2. 1. Basic Curvelet Relations

Firstly, let us define some symbols. In curvelet space, x shows spatial variable, ω is frequency domain variable and r and θ are polar coordinates in the frequency domain. The transform process starts with two windows $F(r)$ and $G(t)$ which are called radial and angular windows, respectively. F is positive real value in the range $r \in (1/2, 2)$ and G real value in the range $t \in [-1, 1]$. These windows always obey the following conditions [12]:

$$\sum_{j=-\infty}^{\infty} F^2(2^j r) = 1 \quad r \in (3/4, 3/2) \quad (2)$$

$$\sum_{l=-\infty}^{\infty} G^2(t-l) = 1 \quad t \in (-1/2, 1/2) \quad (3)$$

In the above functions, j and l are scale and location parameters, respectively. For each $j > j_0$ (j_0 is initial

value j) frequency window V_j is defined in the Fourier domain as:

$$V_j(r, \theta) = 2^{-3j/4} F(2^{-j}r) G\left(\frac{2^{\lfloor j/2 \rfloor} \theta}{2\pi}\right) \tag{4}$$

The waveform $\mu_j(x)$ may be defined by using Fourier transform $\hat{\mu}_j(\omega) = V_j(\omega)$. If function μ_j is taken as a mother curvelet, then all curvelets may be obtained at scales 2^{-j} by rotations θ_l and position x_k^{jl} of function μ_j as:

$$\mu_{jlk}(x) = \mu_j(W_{\theta_l}(x - x_k^{jl})) \tag{5}$$

where W_θ is rotation operator by θ radians. Figure 1 shows scale 2^{-j} in continuous-time curvelet transforms, in which rotation and position parameters may be defined as:

$$\theta_l = 2\pi \cdot 2^{-\lfloor j/2 \rfloor} l \quad l = 0, 1, \dots, 2^{\lfloor j/2 \rfloor} - 1 \tag{6}$$

$$x_k^{jl} = W_{\theta_l}^{-1}\left(k_1 2^{-j}, k_2 2^{-j/2}\right), \quad k = (k_1, k_2) \in Z^2 \tag{7}$$

Based on the above parameters, the curvelet coefficients may be theoretically obtained as follows:

$$CT(j, l, k) = \langle I, \mu_{jlk} \rangle = \int_{R^2} I(x) \overline{\mu_{jlk}(x)} dx \tag{8}$$

The digital transform $CT^D(j, l, k)$ is computed for $I(m', n')$ as:

$$CT^D(j, l, k) = \sum_{0 \leq m' < M} \sum_{0 \leq n' < N} I[m', n'] \mu_{jlk}^D[m', n'] \tag{9}$$

In this paper, the superscript D stands for digital format. Therefore, the digital form of μ_{jlk} is defined as:

$$\mu_{jlk}^D(x) = 2^{3j/4} \mu_j^D(W_{\theta_l}(x - x_k^{jl})) \tag{10}$$

$$W_\theta = \begin{pmatrix} 1 & 0 \\ -\tan \theta & 1 \end{pmatrix} \tag{11}$$

$$\theta_l = l \cdot 2^{-\lfloor j/2 \rfloor} \quad l = -2^{\lfloor j/2 \rfloor}, \dots, 2^{\lfloor j/2 \rfloor} - 1 \tag{12}$$

Equation (9) may be re-written in the frequency domain as:

$$CT^D(j, l, k) = IFFT(FFT(I[m', n']) \times FFT(\mu_{jlk}^D[m', n'])) \tag{13}$$

in which $IFFT$ and FFT stand for inverse fast Fourier transform and fast Fourier transform, respectively.

The additional details of Equation (13) may be found in [13].

There are two ways to implement FDCT: wrapping and USFFT method. The fast Fourier transform USFFT method is utilized in this research.

2. 1. 1. Digital Curvelet Transform Via USFFT

The window V_j in continuous-time definition (4) extracts frequencies near $\{2^j \leq r \leq 2^{j+1}\}$ and $\{-\pi \cdot 2^{-j/2} \leq \theta \leq \pi \cdot 2^{-j/2}\}$. These definitions are not compatible with digital transform. As shown in Figure 2, digital curvelet is based on concentric squares while the continuous time curvelet is based on concentric circles [14].

The window V_j^D (digital form of V_j) is defined by F_j^D and G_j^D (digital forms of F_j and G_j) as:

$$V_j^D = F_j^D G_j^D \tag{14}$$

The 2D Discrete Fourier Transform (DFT) for I is calculated as:

$$\hat{I}(m_f, n_f) = \sum_{m=0}^{M-1} \sum_{n=0}^{N-1} I(m, n) e^{-i2\pi \left(\frac{m_f m}{M} + \frac{n_f n}{N}\right)} \tag{15}$$

$$1 \leq m_f \leq M, \quad 1 \leq n_f \leq N$$

where i represents the imaginary number. Then, the FDCT via USFFT is computed as:

$$CTU^D(j, l, k) = \sum_{m_f, n_f} \hat{I}[m_f, n_f - m_f \tan \theta] \times \tag{16}$$

$$V_j^D[m_f, n_f] e^{i2\pi \left(\frac{k_1 m_f}{L_{1,j}} + \frac{k_2 n_f}{L_{2,j}}\right)}$$

where $L_{1,j}$ and $L_{2,j}$ are length and width in $V_j^D[m_f, n_f]$, respectively. Note that $L_{1,j}$ is about 2^j and $L_{2,j}$ is about $2^{j/2}$ [14].

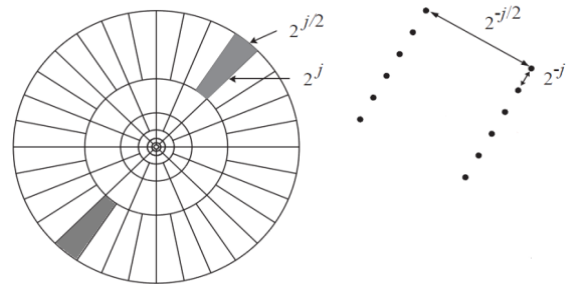


Figure 1. Determination scale curvelet at the frequency plane and spatial Cartesian

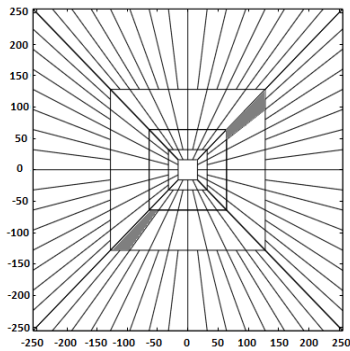


Figure 2. The figure curvelet the basic digital tiling

2. 2. Description of Mapping Function Now, the nonlinear function is constructed based on curvelet coefficients to improve the performance of the detection. For this purpose, let C' as defined in (17) show the mentioned function. In this equation, c is curvelet coefficient and p determines degree of nonlinearity. Further, s_1, s_2, s_3 define the weights which should be assigned to each portion of function to perform some modifications to obtain more appropriate curvelet components. Here, d regulates the coefficient modification interval. Also, z and q are defined as (18) and (19), respectively. These parameters are defined according, firstly the noise standard deviation to avoid from the noise implication, and secondly the maximum value of coefficients [15].

$$C'(c_{mn}(j,l,k)) = \begin{cases} s_1 \left(\frac{z}{q}\right)^p & \text{if } |c_{mn}(j,l,k)| < dq \\ s_2 \left(\frac{z}{|c_{mn}(j,l,k)|}\right)^p & \text{if } dq \leq |c_{mn}(j,l,k)| < z \\ s_3 & \text{if } |c_{mn}(j,l,k)| \geq z \end{cases} \quad (17)$$

$$z = s(\max(c_{jk}) - q) \quad (18)$$

$$q = \sqrt{\frac{\pi}{2}} \frac{1}{6(k-2)(l-2)} \sum |I_{m'n'} * \Delta| \quad (19)$$

$$\Delta = \begin{bmatrix} 1 & -2 & 1 \\ -2 & 4 & -2 \\ 1 & -2 & 1 \end{bmatrix}$$

In the above equations, the image I is divided into multiple blocks of a pre-defined size (for example (32×32)), and $*$ represents the time domain convolution. For better interpretation of the proposed algorithm the analysis of the mapping function has been shown in Figures 3 and 4 as evaluation of its sensitivity due to effective parameters p and z , respectively.

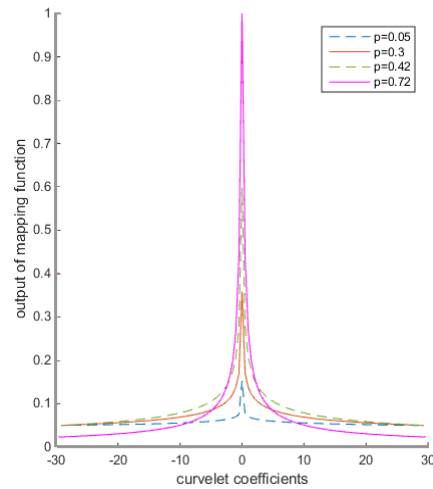


Figure 3. The sensitivity of the mapping function against p parameter in Equation (17)

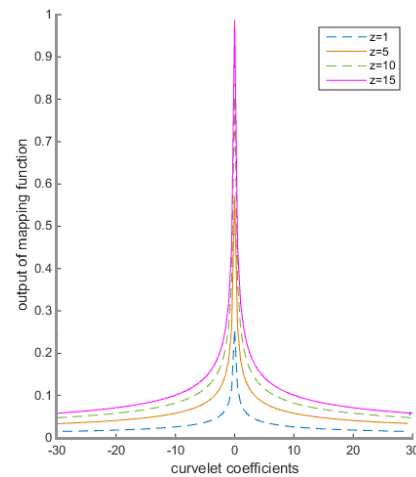


Figure 4. The sensitivity of the mapping function against z parameter in Equation (17)

By applying inverse curvelet transform on the mapped curvelet components and finally using Entropy Based Level Set (EBLS) method, the dependency of each pixel to root or background is obtained which leads to the boundary of root as described in our previous research [11]. Figure 5 offers Implementation scheme for the proposed algorithm in the form of pseudo code.

3. TESTS AND RESULTS

The proposed algorithm was applied to the real data set which is composed of minirhizotron images in which half of the images contain variety of roots and the residue are no-root images including background, bright objects and dead roots.

<p><i>Detection Procedure</i></p> <p><i>For each minirhizotron image</i></p> <ul style="list-style-type: none"> - Calculating digital curvelet transform - Modification sub-band curvelet coefficients using mapping function - Adapting parameters of mapping function with current curvelet components - Applying inverse curvelet transform - Define hypothesis testing equation for each pixel of minirhizotron image - Applying primary edge detector on image to perform initial estimation of boundary - Optimizing energy function based on level set concept and to obtain final boundaries of roots <p><i>End of detection procedure</i></p>

Figure 5. Pseudo code the proposed algorithm

TABEL 1. Specifications of examined minirhizotron images and root

Specification of Images	Value	Specification of Roots	Value
Number of tested images	50 frames	Plant Species	Magnolia and Peach
Average contrast	19%	Min and Max length of roots	60 , 490 Pixels
Frame size (pixels)	480*640 pixels	Min and Max width of roots	12 , 33 Pixels

TABEL 2. Parameters of mapping function

Parameter	value	Parameter	value
s_1	0.1	d	1.25
s_2	0.05	s	1.1
s_3	1	p	0.05

Table 1 shows some important parameters of the test images (e.g. number, contrast and size) and some important parameters of roots (e.g. type, length and width). More details may be found in [7, 11]. The proposed algorithm is implemented using Matlab 2014 and is applied to the above data set. To evaluate the performance of the proposed algorithm, the EBLs method [11], Curvelet Transform Without Mapping (CTWM), Entropy Thresholding Algorithm (ETA) [7] and Gabor Filter [16] were implemented and applied to the data set as same as our proposed scheme. A brief description of some results which have been obtained from all examined methods have been presented in

graphical form in this section. Full statistics of the results will be discussed in Section 4.

Table 2 shows the parameters of the mapping function which led to the best results in this research.

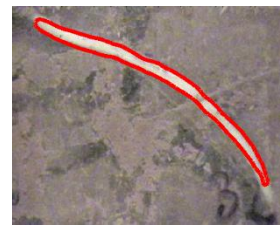
3. 1. First Scenario

In the first scenario, algorithms are applied to images which contain Root. Figure 6 shows the results of the examined algorithms that have been imposed on Figure (6-a). Figure (6-b) shows hand-labeled version of Figure (6-a). Figure (6-c) shows the result from testing EBLs on the raw image *I* in which the root has been divided into two parts. Figures (6-d), (6-e) and (6-f) show that results obtained from ETA, Gabor Filter and CTWM, respectively. These algorithms have divided the root into two parts; further, a number of root pixels were omitted. Finally, Figure (6-g) shows the result of applying the proposed method in which the root is extracted without being divided or having extra pixels. Figure 7 shows another test on one-root images which has lower contrast than those shown in Figure (6-a). As shown, EBLs, ETA, Gabor Filter and CTWM have divided the root into two or more parts. Further, a significant number of root pixels have been loosed. The proposed method have extracted the root without being divided or having extra pixels as shown in Figure (7-g).

Figure 8 shows another type of results in which the two-root pictures have been examined. Figures (8-c), (8-e) and (8-f) show the results obtained from EBLs, Gabor Filter and CTWM, respectively. Although all of these algorithms have extracted two roots existing in Figure (8-a), but a considerable number of pixels have been ignored. As shown in Figure (8-d), ETA also has extracted both roots, but the first root has been divided into three parts and many pixels belonging to the second root has been lost. Figure (8-g) shows that the proposed algorithm has extracted both roots better than the other examined algorithms. However, still the second root has been detected incompletely.

3. 2. Second Scenario

Presence of some bright objects and existing some dead roots in the background of minirhizotron images - which may be identified as root- may be a great challenge in the root detection procedure. Based on this fact, in the second scenario, those images which contain any roots were examined. Figure (9-a) shows an example of these images. Figures (9-d), (9-e) and (9-f) shows the results of applying ETA, Gabor Filter and CTWM that has led to some false detections. However, Figure (9-c) and (9-g) show no false detections as the result of applying EBLs as well as the proposed method.



(g)



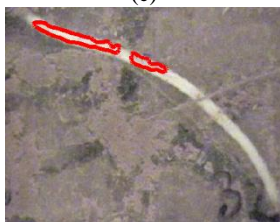
(a)



(b)



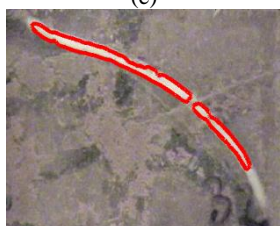
(c)



(d)



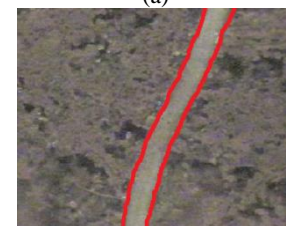
(e)



(f)



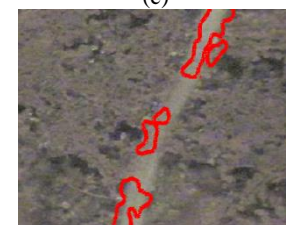
(a)



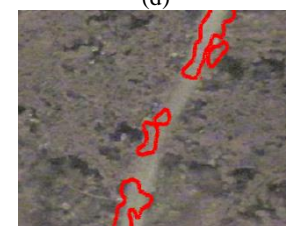
(b)



(c)



(d)



(e)

Figure 6. (a) - A One-Root minirhizotron image, (b) - Hand-Labeled image, detection results by using (c) - EBLs, (d) - ETA,(e) - Gabor Filter, (f) - CTWM and (g) - The Proposed Algorithm

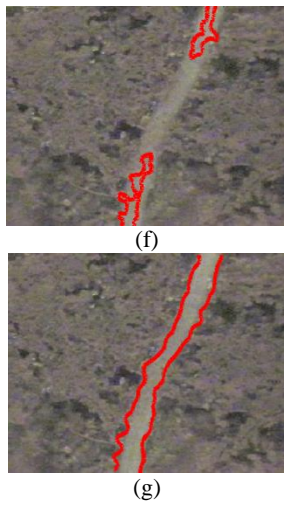


Figure 7. (a) - A One-Root minirhizotron image, (b) - Hand-Labeled image, detection results by using (c) - EBLs, (d) - ETA,(e) - Gabor Filter, (f) - CTWM and (g) - The Proposed Algorithm

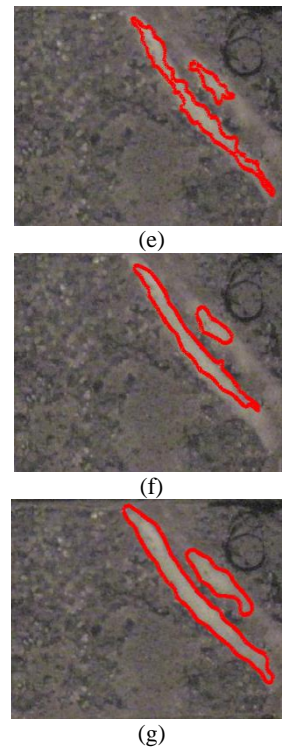
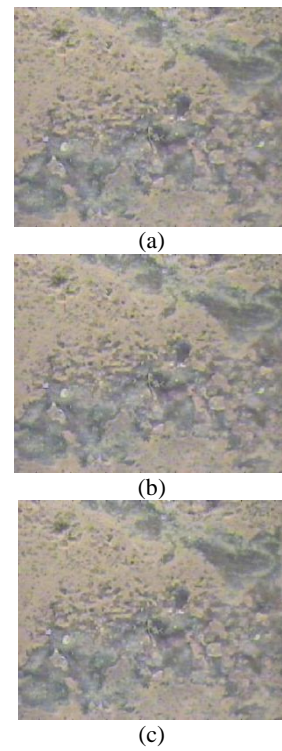
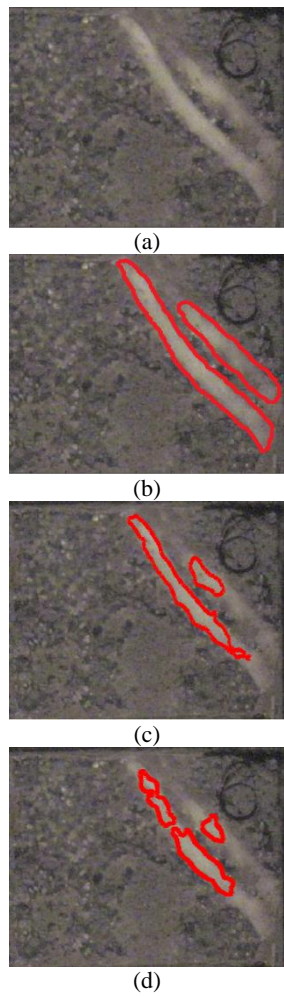


Figure 8. (a) - A Two-Root minirhizotron image, (b) - Hand-Labeled image, detection results by using (c) - EBLs, (d) - ETA,(e) - Gabor Filter, (f) - CTWM and (g) - The Proposed Algorithm



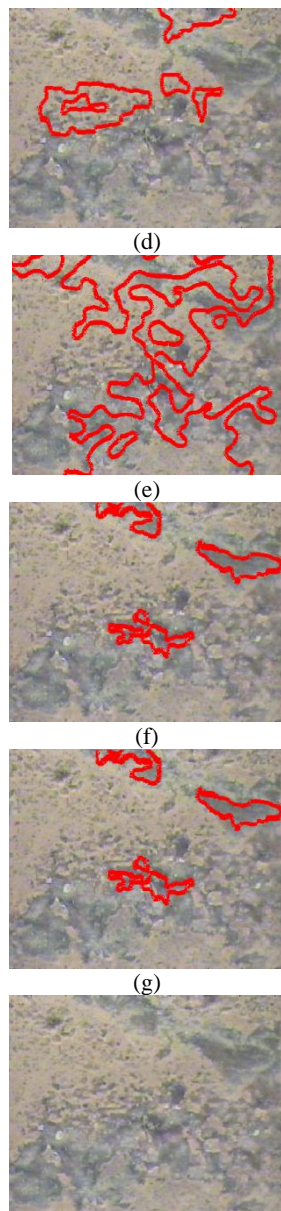


Figure 9. (a) - A No-Root minirhizotron image, (b) - Hand-Labeled image, detection results by using (c) - EBLS, (d) - ETA, (e) - Gabor Filter, (f) - CTWM and (g) - The Proposed Algorithm

4. PERFORMANCE MEASURES

The proposed algorithm, EBLS, CTWM, ETA and Gabor Filter were applied to real data. Then, false positive rate (FPR) and true positive rate (TPR) parameters were obtained for several examined methods to compare the results. Equations (20) and (21) show the calculation of two above parameters them; true positive (TP) shows the number of correctly identified roots. True negative (TN) shows those objects which were

correctly rejected. False positive (FP) shows false detections and false negative (FN) is defined as number of missed roots. The first parameter, called TPR is the probability of detecting pixels appointed to the root and was estimated as:

$$TPR = \frac{TP}{TP+FN} \tag{20}$$

Furthermore, FPR is the statistics of pixels being related to the false roots and was estimated as:

$$FPR = \frac{FP}{FP+TN} \tag{21}$$

Figure 10 shows a curve called receiver operating characteristic (ROC) which shows the advantage of the proposed method compared to other four methods in terms of parameter diagnosis changes of FPR versus TPR. For simpler interpretation, FPR=0% and TPR=100% has been shown as ideal values for false detection and detection probabilities in Table 3.

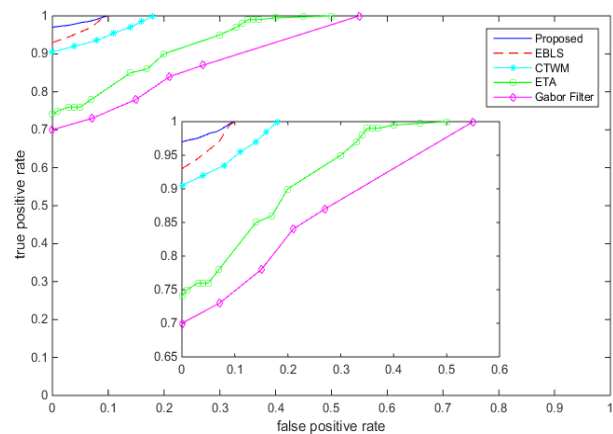


Figure 10. ROC curves obtained for the proposed (solid line-blue), EBLS (dashed line-red), CTWM (star line-cyan), ETA (square line- green) and Gabor Filter (diamond line-magenta)

TABLE 3. Comparison of the performances of examined algorithms

Examined Methods	TPR for FPR=0%	FPR for TPR=100%	TPR for FPR=5%	FPR for TPR=90%
Proposed	0.97	0.098	0.984	0
EBLS	0.93	0.1	0.958	0
CTWM	0.905	0.18	0.923	0
ETA	0.74	0.5	0.765	0.2
Gabor Filter	0.7	0.55	0.723	0.33

The performances of algorithms may be compared using other arbitrary thresholds for acceptable FPR and TPR by using Figure 10 in the same manner.

As shown in Table 3, the detection rate obtained in the proposed algorithm was 4, 6.5, 23 and 27% better than EBLs, CTWM, ETA and Gabor Filter methods, respectively, in zero false detection rate. Also, this table shows the FPR of the proposed algorithm to be 0.2, 8.2, 40.2 and 45.2% less than EBLs, CTWM, ETA and Gabor Filter methods, respectively, when the detection rate has been complete.

A more realistic comparison has been performed in Table 3 for more actual values of TPR and FPR (e.g. 9 and 5%, respectively) which again leads to superiority of the proposed algorithms in contrast to its alternatives.

As shown in Figure 10, an optimum point with FPR=7% has been considered for the proposed method and was compared with alternative algorithms. The proposed algorithm gives TPR value equal to 98.7% when the false positive rate had been 7%, whereas, the methods EBLs, CTWM, ETA and Gabor Filter have had detection rates equal to 97, 93, 78 and 73%, respectively, in the same FPR.

5. CONCLUSION

In this paper a new method was introduced for separating root from other parts in minirhizotron images. In the proposed method, firstly based on its scaling and directionality, the digital curvelet transform was utilized to make a mapping function. Adapting key parameters of this function according to curvelet sub-bands led to improve detection procedure by magnifying weak ridges without increasing false edges which are caused due to noise. Two different scenarios were considered to evaluate the performance of the proposed algorithm. In the first scenario one or two root images were analyzed while in the second one the no-root images were tested. For better interpretation, the tests were also carried on four alternative methods (e.g. EBLs, CTWM, ETA and Gabor Filter) and the results were compared by using their ROC. The results show that the proposed algorithm has extracted roots at least 4% higher than EBLs which was the best among other examined methods in presence of a typically false detection rate equal with 0%. Furthermore, it was observed that false detection rate of the proposed algorithm has been at least 0.2% less than the best of the full detection rate (i.e.100%). These results showed that better root detection capability of the proposed algorithm has not led to more false detections.

6. REFERENCES

- Hodge, A., Berta, G., Doussan, C., Merchan, F. and Crespi, M., "Plant root growth, architecture and function", *Plant and soil*, Vol. 321, No. 1-2, (2009), 153-187.
- Dowdy, R., Smucker, A., Dolan, M. and Ferguson, J., "Automated image analyses for separating plant roots from soil debris elutriated from soil cores", *Plant and soil*, Vol. 200, No. 1, (1998), 91-94.
- Himmelbauer, M., "Estimating length, average diameter and surface area of roots using two different image analyses systems", *Plant and soil*, Vol. 260, No. 1-2, (2004), 111-120.
- Silva, D.D. and Beeson, R.C., "A large-volume rhizotron for evaluating root growth under natural-like soil moisture conditions", *HortScience*, Vol. 46, No. 12, (2011), 1677-1682.
- Munoz-Romero, V., Benítez-Vega, J., López-Bellido, L. and López-Bellido, R.J., "Monitoring wheat root development in a rainfed vertisol: Tillage effect", *European Journal of Agronomy*, Vol. 33, No. 3, (2010), 182-187.
- Hassanpour, H. and Yousefian, H., "An improved pixon-based approach for image segmentation", *International Journal of Engineering-Transactions A: Basics*, Vol. 24, No. 1, (2010), 25-35.
- Zeng, G., Birchfield, S.T. and Wells, C.E., "Detecting and measuring fine roots in minirhizotron images using matched filtering and local entropy thresholding", *Machine Vision and Applications*, Vol. 17, No. 4, (2006), 265-278.
- Zeng, G., Birchfield, S.T. and Wells, C.E., "Automatic discrimination of fine roots in minirhizotron images", *New Phytologist*, Vol. 177, No. 2, (2008), 549-557.
- Nater, E.A., Nater, K.D. and Baker, J.M., "Application of artificial neural system algorithms to image analysis of roots in soil, i. Initial results", *Geoderma*, Vol. 53, No. 3, (1992), 237-253.
- Zeng, G., Birchfield, S.T. and Wells, C.E., "Rapid automated detection of roots in minirhizotron images", *Machine Vision and Applications*, Vol. 21, No. 3, (2010), 309-317.
- Shojaedini, S. and Heidari, M., "A new method for root detection in minirhizotron images: Hypothesis testing based on entropy-based geometric level set decision", *Ij*, Vol. 1, No. 1, (2013).
- Candes, E.J. and Donoho, D.L., "'Curvelets multi-resolution representation, and scaling laws, wavelet applications'", in *Signal and Image Processing VIII*. Vol. 4119, (2000 of Conference).
- Zhang, D., Wong, A., Indrawan, M. and Lu, G., "Content-based image retrieval using gabor texture features", in *IEEE Pacific-Rim Conference on Multimedia*, University of Sydney, Australia. (2000), 91-110.
- Candes, E., Demanet, L., Donoho, D. and Ying, L., "Fast discrete curvelet transforms", *Multiscale Modeling & Simulation*, Vol. 5, No. 3, (2006), 861-899.
- Zhao, Z.-b., Yuan, J.-s., Gao, Q. and Kong, Y.-h., "Wavelet image de-noising method based on noise standard deviation estimation", in *Wavelet Analysis and Pattern Recognition, 2007. ICWAPR'07. International Conference on, IEEE*. Vol. 4, (2007), 1910-1914.
- Zhang, D., Islam, M.M., Lu, G. and Sumana, I.J., "Rotation invariant curvelet features for region based image retrieval", *International journal of computer vision*, Vol. 98, No. 2, (2012), 187-201.

Novel Automated Method for Minirhizotron Image Analysis: Root Detection Using Curvelet Transform

H. Rahmanzadeh^a, S. V. Shojaedini^b

^a Department of Electrical, Biomedical and Mechatronics Engineering, Qazvin Branch, Islamic Azad University, Qazvin, Iran.

^b Department of Electrical Engineering and Information Technology, Iranian Research Organization for Science and Technology, Iran.

PAPER INFO

چکیده

Paper history:

Received 06 December 2015

Received in revised form 14 February 2016

Accepted 03 March 2016

Keywords:

Minirhizotron Images

Root Detection

Curvelet Sub-Bands

Mapping Function

در این مقاله یک روش جدید برای تفکیک ریشه‌ها و پس‌زمینه در تصاویر مینی رایزتروتن بر اساس تبدیل کرولت دیجیتال آنها معرفی می‌شود. در روش پیشنهادی، یک نگاهت غیرخطی به زیر باندهای کرولت اعمال شده و به دنبال آن با استفاده از مفهوم بهینه سازی انرژی، مرزهای ریشه‌ها آشکار می‌شوند. تبدیل کرولت به دلیل نمایش پراکندگی بهتر و دارا بودن ویژگی‌های جهتی بیشتر، قابلیت بالاتری را در تشخیص ریشه‌ها با جهت‌ها و کنتراست مختلف در مقایسه با روش‌های موجود از خود نشان می‌دهد. علاوه بر این، تطبیق پارامترهای تابع نگاهت بر اساس ضرایب کرولت موجود، هم از نظر بزرگنمایی لبه‌های ضعیف و هم از نظر سازگاری بهتر با تصاویر متنوع مینی رایزتروتن بسیار سودمند واقع می‌شود. عملکرد روش پیشنهادی با اعمال آن بر تصاویر گوناگون مینی رایزتروتن در قالب دو سناریوی مختلف ارزیابی می‌شود. در سناریوی اول، تصاویر مورد آزمون شامل ریشه‌اند، در حالی که سناریوی دوم متعلق به تصاویر بدون ریشه است که احتمال تشخیص نادرست را افزایش می‌دهند. نتایج به دست آمده نشان می‌دهند که روش پیشنهادی در شرایطی که هیچ تشخیص نادرستی انجام نشود، به نرخ آشکارسازی ۴ تا ۲۷ درصد بهتر از روش‌های رقیب دست می‌یابد. به علاوه، ملاحظه می‌شود که تخمین مشخصات بهتر ریشه‌ها توسط روش پیشنهادی موجب افزایش نرخ آشکارسازی غلط نسبت به سایر روش‌های آزموده شده، نمی‌گردد.

doi: 10.5829/idosi.ije.2016.29.03c.08